High dimensional stability of $LiCoMnO_4$ as positive electrodes operating at high voltage for lithium-ion batteries with a long cycle life

Kingo Ariyoshi, Hiroya Yamamoto and Yusuke Yamada

ARIYOSHI, K., YAMAMOTO, H., & YAMADA, Y. (2018). High dimensional stability of $LiCoMnO_4$ as positive electrodes operating at high voltage for lithium-ion batteries with a long cycle life. *Electrochimica Acta.* 260, 498-503. doi:10.1016/j.electacta.2017.12.064

Contents lists available at ScienceDirect

Electrochimica Acta

journal homepage: www.elsevier.com

High dimensional stability of $LiCoMnO_4$ as positive electrodes operating at high voltage for lithium-ion batteries with a long cycle life

Kingo Ariyoshi*, Hiroya Yamamoto, Yusuke Yamada**

Department of Applied Chemistry and Bioengineering, Graduate School of Engineering, Osaka City University, 3-3-138 Sugimoto, Sumiyoshi-ku, Osaka, 558-8585, Japan

ARTICLE INFO

Article history:
Received 30 August 2017
Received in revised form 6 December 2017
Accepted 10 December 2017
Available online xxx

Keywords:
Lithium-ion battery
Lithium cobalt manganese oxide
Dimensional stability

ABSTRACT

Dimensionally stable $LiCoMnO_4$ having a spinel-framework structure was developed as a positive electrode of lithium-ion batteries with a long cycle life. Well-crystallized $LiCoMnO_4$ prepared by a two-step solid-state reaction shows large rechargeable capacity of 120 mAh g^{-1} at high operating voltage of 5 V. Ex-situ XRD measurements of the $LiCoMnO_4$ revealed small change in the cubic lattice parameter (ca. 0.7%) during charge and discharge. Change in electrode thickness of $LiCoMnO_4$ measured by using a precision dilatometer is accordance with the change in the cubic lattice parameter. The $LiCoMnO_4$ electrode showed high dimensional stability compared with other $LiMn_2O_4$-based materials having a spinel-framework structure.

ca (in Italic font)

1. Introduction

During the past three decades, lithium insertion materials used for electrodes in lithium-ion batteries have been developed to improve battery performances towards high voltage, large capacity, a cycle life, etc. In recent years, cycleability closely related to the cycle life of a lithium-ion battery is regarded as one of the most important performances for applications of lithium-ion batteries expanded into automobile and stationary uses. One of the most crucial factors affecting cycleability of lithium insertion materials is the fracture formation [1–5] resulted from expansion and contraction of the materials during lithium insertion and extraction reactions [6–8]. An ideal lithium insertion material for long-life applications is a zero-strain insertion material in which no dimensional change during lithium insertion and extraction reactions. For example, a $Li[Li_{1/3}Ti_{5/3}]O_4$ (LTO)/$LiCo_{1/3}Ni_{1/3}Mn_{1/3}O_2$ cell shows good cycleability [9], because LTO is the zero-strain material [10–12] and $LiCo_{1/3}Ni_{1/3}Mn_{1/3}O_2$ exhibits no lattice volume change in the operating voltage range below 4.4 V vs. Li [13]. Employment of zero-strain materials for both positive and negative electrodes provides lithium-ion batteries, which can avoid the swelling or an internal short circuit problem.

delete ","

Dimensional stability of lithium insertion materials is important not only for improving a cycle life but also for developing all solid-state batteries. Recently, all solid-state lithium-ion batteries have been widely and extensively investigated as next-generation batteries [14,15]. In all solid-state lithium-ion batteries, dimensional stability of electrode materials is highly required, because large dimensional change in electrode materials may result in destruction of interface between an electrode and a solid electrolyte, leading to loss of electrochemical contacts during cycling. Thus, lithium-insertion materials with high dimensional stability are regarded as a key material for developing all solid-state batteries to deliver full potentials, such as excellent cycleability and high reliability [16]. However, only a few lithium insertion materials have reported to possess high dimensional stability, because dimensional change in the crystal lattice is hardly controlled without lowering electrochemical performance, such as operating voltage and reversible capacity.

Among $LiM_xMn_{2-x}O_4$ (M: 3d-transition metals) known as high voltage positive electrode materials, $LiCo_xMn_{2-x}O_4$ showed the smallest change in a lattice parameter during Li insertion reaction [17]. Increasing the Co content resulted in decrease of the lattice parameter during lithium insertion reaction. This result indicates that $LiCoMnO_4$ is attractive for dimensionally stable electrode with good cycleability, because $LiCoMnO_4$ has the highest Co content in $LiCo_xMn_{2-x}O_4$. However, discharge capacity of $LiCoMnO_4$ reported so far is limited to be less than 100 mAh g^{-1} due to low coulombic efficiency and rapid capacity fading caused by high operating voltage at 5 V [17–19].

Increasing the degree of crystallinity has been reported to improve cycleability of 5 V materials [20–22]. Highly crystalline $Li[Ni_{1/2}Mn_{3/2}]O_4$ (LiNiMO) known as a 5 V material was obtained by the two-step solid-state reaction. The highly crystalline LiNiMO with octahedral particles with smooth (111) facets [20] showed high cycleability with negligibly small capacity loss (<4% after 250 cycles) [21] and low power fading (ca. 10% after the continuous 200,000 cycles) even at the high operating voltage of 5 V [22]. High crystallinity with smooth crystal facets can enhance cycleability of other high-voltage materials, although resulting in reduction of effective surface area.

"ca." (in Italic font)

"$Li[Ni_{1/2}Mn_{3/2}]O_4$" should be in the same line.

* Corresponding author.
** Corresponding author.
Email addresses: ariyoshi@a-chem.eng.osaka-cu.ac.jp (K. Ariyoshi); ymd@a-chem.eng.osaka-cu.ac.jp (Y. Yamada)

https://doi.org/10.1016/j.electacta.2017.12.064
0013-4686/

In this paper, we prepared well-crystallized $LiCoMnO_4$ by a two-step solid-state reaction to achieve discharge capacity higher than 100 mAh g^{-1} and to examine dimensional stability. $LiCoMnO_4$ prepared by a two-step solid-state reaction shows high operating voltage at 5 V with reversible capacity larger than 100 mAh g^{-1}. Dimensional stability of $LiCoMnO_4$ was examined by ex-situ XRD in terms of lattice parameters and by dilatometry in terms of electrode thickness. Cycleability of the LTO/$LiCoMnO_4$ cell was confirmed in 50 cycles.

2. Experimental

ca (in Italic font)

Chemical

2.1. Material synthesis and characterization

$LiCoMnO_4$ was prepared by a two-step solid-state reaction consisting of crystallization at high temperature and oxidation at relatively low temperature for long time [20]. Staring materials, $LiOH{\cdot}H_2O$ and a cobalt manganese double hydroxide (MX-096, Tanaka ~~chemical~~ Corp., Ltd), were heated at 900 °C for 12 h for crystallization, and then cooled at 700 °C for 24 h, 650 °C for 24 h, and 600 °C for ca. 300 h for oxidation. Powder X-ray diffraction patterns were measured with an X-ray diffractometer (XRD-6100, Shimadzu Co. Ltd. Japan) equipped with ~~graphite~~ monochromator, using Fe *Kα* radiation (40 kV and 15 mA) at a scan rate of 0.5° per minute from 9 to 104°. The cubic lattice parameter of $LiCoMnO_4$ was calculated by a least-squares method using 9 diffraction lines with a standard deviation of ±0.1% (less than ±0.005 Å in $LiCoMnO_4$ with a = ca. 8.06 Å).

a graphite

2.2. Electrochemical measurements

To prepare electrodes, black viscous slurry consisting of 88 wt% of $LiCoMnO_4$ or LTO, 6 wt% of acetylene black, and 6 wt% of polyvinylidene fluoride dispersed in *N*-methyl-2-pyrrolidone (NMP) was cast onto an aluminum foil. NMP was evaporated at 80 °C for 1 h under vacuum, and the electrode was dried under vacuum at 150 °C overnight. Finally, the electrode was punched out to form a disk (16.0 mm dia.). An LTO electrode or lithium metal was used as a negative electrode. The electrolyte used was 1 M $LiPF_6$ dissolved in ethylene carbonate/dimethyl carbonate (3/7 by volume) solution (Kishida Chemical Co. Ltd., Japan). The procedure for constructing Li/$LiCoMnO_4$ or LTO/$LiCoMnO_4$ cells was reported elsewhere [23]. Electrochemical tests were carried out with a battery cycler (Battery Laboratory System, KEISOKUKI CENTER Co. Ltd., Japan). Change in thickness of the positive electrode containing $LiCoMnO_4$ in the lithium-ion cell was examined by using a dilatometer [23]. A dilatometer consists of a main body and a flexible bag cell. The change in thickness of the cell is transmitted via a spindle to a linear voltage displacement transducer (AT2-51, Keyence Co. Ltd., Japan) tightly fixed to the main body on the top of a spindle. The transducer connected to an amplifier (AT2-301, Keyence Co. Ltd.) converts a displacement signal in μm to a voltage signal in mV. A range of displacement to be able to record is ±0.5 mm corresponding to ±5 V in voltage output with a zero-shift allowance of ±25 mV. In order to calibrate a full system, a voltage signal from the amplifier is measured by inserting a stainless-steel sheet or plate accurately measured by a micrometer. The determined value is that one-micron displacement corresponds to 10 mV, i.e., 0.1 μm mV^{-1}.

3. Results and discussion

Charge and discharge curves of a Li/$LiCoMnO_4$ cell operated at 0.25 mA cm^{-2} in the voltage range from 3.0 to 5.4 V are shown in Fig. 1. The weight and thickness of the $LiCoMnO_4$ electrode in the cell were 37.5 mg and 110 μm, respectively. Charge and discharge curves in the initial 3 cycles except for the first charge showed steady-state voltage profiles. Operating voltage of the $LiCoMnO_4$ was 5 V over the entire capacity range and the observed capacity at 4 V was quite small (<10 mAh g^{-1}). Average operating voltage of the $LiCoMnO_4$ was 5.0 V with charge and discharge capacities of 140 and 120 mAh g^{-1}, respectively. The discharge capacity of 120 mAh g^{-1} corresponds to 83% of the theoretical capacity of 145 mAh g^{-1} calculated from the formula weight of $LiCoMnO_4$ by assuming one-electron transfer per a formula unit. Although high operating voltage of the $LiCoMnO_4$ (5.0 V) resulted in large self-discharge due to an electrolyte decomposition, the Li/$LiCoMnO_4$ cell showed large discharge capacity (120 mAh g^{-1}). Well-crystallized $LiCoMnO_4$ showed relatively high coulombic efficiency (86%) even when charge-end voltage was set to 5.4 V. The large discharge capacity and high coulombic efficiency for $LiCoMnO_4$ can be achieved by developing the particles with smooth surface as shown in the inset of Fig. 1. From these results, well-crystallized $LiCoMnO_4$ is suitable for examining a dimensional stability together with a reaction mechanism. Very small but not negligible capacity at 4 V region shown in Fig. 1 is an obvious sign for the presence of Mn^{3+} ions in $LiCoMnO_4$ associated with oxygen deficiency. $LiCoMnO_4$ prepared at high temperature released oxygen from the crystal lattice together with transformation to rock-salt phase from spinel phase [24]. $LiCoMnO_4$ oxidized at 600 °C for more than 1 week showed the discharge capacity of 5 mAh g^{-1} at 4 V region, indicating that the $LiCoMnO_4$ was slightly oxygen-deficient. Although the $LiCoMnO_4$ prepared by the two-step solid-state reaction has a small deviation from the stoichiometry, the electrochemical reaction of the $LiCoMnO_4$ proceeds as follows: $LiCo^{3+}Mn^{4+}O_4 \rightarrow \square Co^{4+}Mn^{4+}O_4 + Li^+ + e^-$, because of large discharge capacity at 5 V region close to the theoretical value with less than 5% of the total capacity at 4 V region.

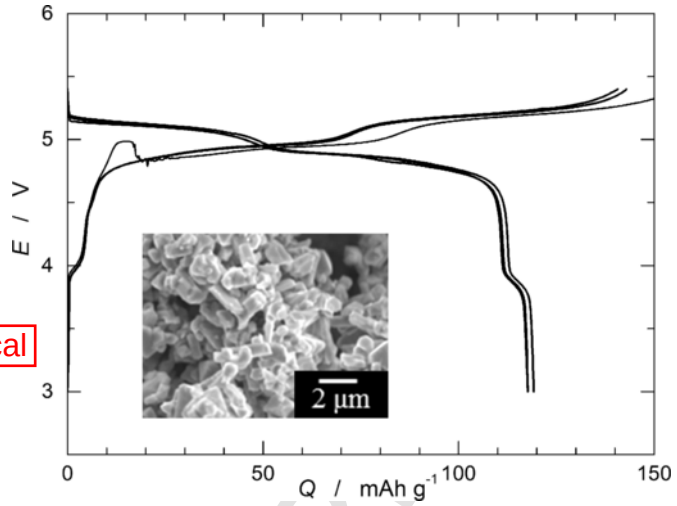

Fig. 1. Initial 3 cycles of charge and discharge curves of a Li/$LiCoMnO_4$ cell operated at 0.25 mA cm^{-2} in the voltage range from 3.0 to 5.4 V. The weight and thickness of the $LiCoMnO_4$ electrode were 37.5 mg and 110 μm, respectively. Inset: an SEM image of $LiCoMnO_4$ particles.

Change in the lattice dimension of $LiCoMnO_4$ during lithium insertion reaction was confirmed by ex-situ XRD measurements. For the ex-situ XRD measurements, Li/$LiCoMnO_4$ cells were cycled for 2 cycles, and then the cells were discharged to several state-of-discharges after fully charged to 5.4 V (Fig. 2). Discharge curves of the cell for the ex-situ XRD measurements were merged into a single curve, and open-circuit voltages of the cells were located above the discharge voltage. The ex-situ XRD measurements were carried out

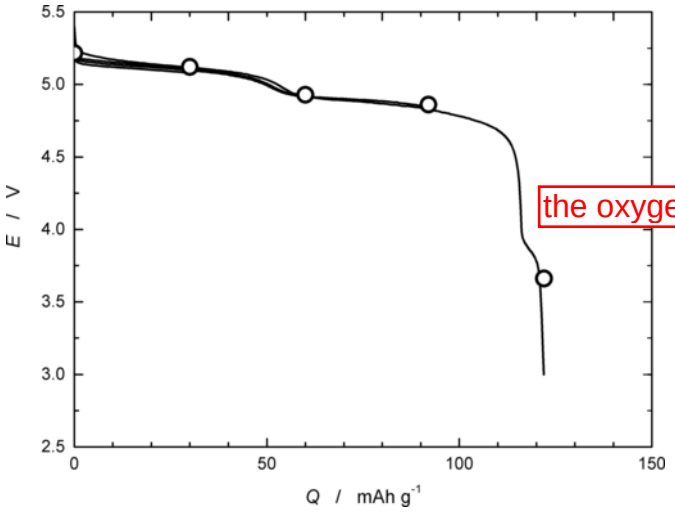

Fig. 2. Discharge curves of Li/$LiCoMnO_4$ cells used for ex-situ XRD measurements. Open circles indicate open-circuit voltages before disassembling the cells. The Li/$LiCoMnO_4$ cells were charged and discharged for 2 cycles, and then discharged at a rate of 0.25 mA cm^{-2} after fully charged to 5.4 V.

for $LiCoMnO_4$ electrodes during discharge in order to avoid ambiguity of state-of-charge of $LiCoMnO_4$, because state-of-charge during charge is difficult to be determined due to the low coulombic efficiency. Fig. 3 shows XRD patterns of $LiCoMnO_4$ electrodes at several state-of-discharges. The ex-situ XRD measurements were performed for the $LiCoMnO_4$ electrodes charged and discharged in the cell. The electrodes taken out from the cell were sealed with a polyethylene film to avoid reactions with moisture in air. The XRD pattern of pristine $LiCoMnO_4$ was similar to that of normal spinel compounds, $Li[Me_2]O_4$ (Me = transition metals), so that the crystal structure of $LiCoMnO_4$ was identified as $Li[CoMn]O_4$ with a space group symmetry of *Fd3(_)m* in which Co and Mn ions and Li ions occupied octahedral 16d and tetrahedral 8a sites, respectively, in a cubic close-packed oxygen array. A cubic lattice parameter of $LiCoMnO_4$ was calculated to be 8.058 Å. The lattice parameter of $LiCoMnO_4$ increases with increasing ~~oxygen~~ deficiency due to the formation of Mn^{3+} [24]. The lattice parameter of the well-crystallized $LiCoMnO_4$ prepared by the two-step solid-state reaction is almost the same as those previously reported for $LiCoMnO_4$ [17–19,24].

The XRD patterns of $LiCoMnO_4$ at different discharge capacities showed insignificant difference in the number, width, and intensity of the diffraction lines. However, diffraction lines shifted toward higher diffraction angles by decreasing the discharge capacity, suggesting that the lithium insertion processes of $LiCoMnO_4$ proceed in a single-phase reaction. The lattice parameter of $LiCoMnO_4$ at the fully discharged state was the same as that at the initial state. No significant difference in the XRD patterns between pristine material and fully discharged electrode ~~was observed, indicating~~ that the change in the crystal structure of $LiCoMnO_4$ is highly reversible during lithium insertion reaction. Cubic lattice parameters of $LiCoMnO_4$ with different discharged conditions were plotted against the discharged capacity in mAh g^{-1} based on $LiCoMnO_4$ weight (Fig. 4). The cubic lattice parameter of $LiCoMnO_4$ increases linearly from 8.00 to 8.06 Å by increasing discharge capacity, which is almost the same as that reported in the paper [17,24]. The change in lattice dimension is 0.06 Å, corresponding to *ca*. 0.7% change in the lattice parameter of the pristine $LiCoMnO_4$. Change in the unit-cell volume was estimated to be 2.2%, which was one-third of those reported for other lithium insertion materials having spinel-framework structures, e.g., $LiMn_2O_4$ (*ca*. 7%) [25] and $Li[Ni_{1/2}Mn_{3/2}]O_4$ (*ca*. 6%) [20].

The lattice parameter of cubic spinel is directly related to bond length between transition metal ions and oxygen ions at the octahedral sites as well as oxygen positional parameter of *u* at 32e site. Thus, a lithium insertion material with small change in lattice dimension have metal ions with small change in ionic radii and suitable change in oxygen positional parameters during lithium insertion and extraction [11]. The small change in the lattice dimension of Li-

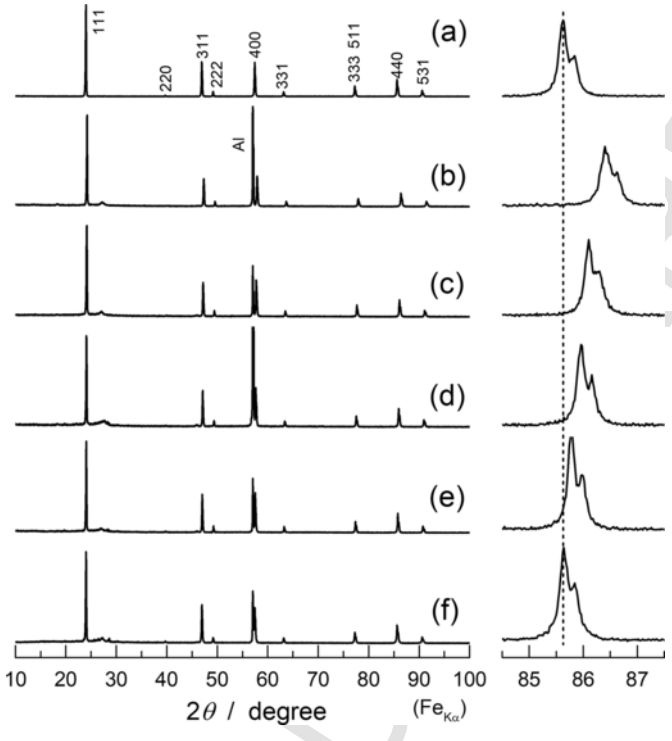

Fig. 3. XRD patterns of (a) pristine $LiCoMnO_4$ and $LiCoMnO_4$ electrodes with discharge capacities of (b) 0 mAh g^{-1}, (c) 30 mAh g^{-1}, (d) 60 mAh g^{-1}, (e) and 90 mAh g^{-1} and (f) 120 mAh g^{-1} after charging to 5.4 V. Right panels are magnification of the 440 diffraction lines. The cubic lattice parameters were (a) 8.058 Å, (b) 8.000 Å, (c) 8.021 Å, (d) 8.033 Å, (e) 8.046 Å and (f) 8.057 Å. Weak diffraction lines between 25 and 30° are attributed to polyethylene film covering the electrodes for ex-situ XRD measurements.

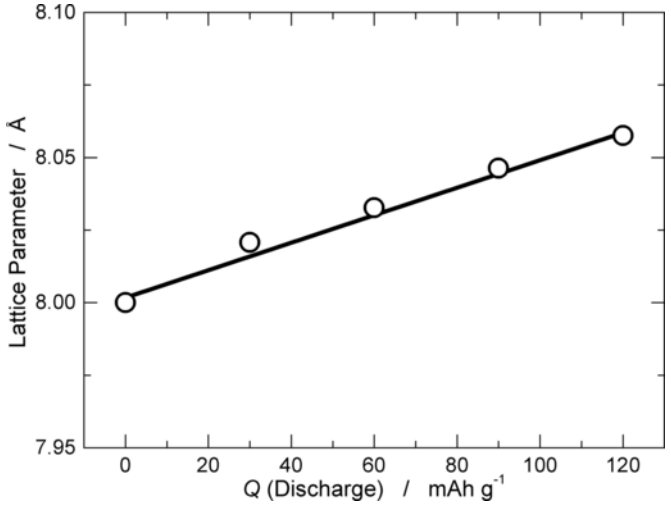

Fig. 4. Change in the lattice parameters as a function of discharge capacity in mAh g^{-1} based on the $LiCoMnO_4$ weight.

Fd–3m ("–" should be on top of "3").

the oxygen

indicates

$CoMnO_4$ compared with those of $LiMn_2O_4$ and LiNiMO is mainly ascribed to the small change in ionic radius of Co^{3+}/Co^{4+} ions. The difference in ionic radius of Co^{3+}/Co^{4+}, Δr (Co^{3+}/Co^{4+}) = 0.015 Å, is significantly smaller than Δr (Mn^{3+}/Mn^{4+}) = 0.115 Å and Δr (Ni^{2+}/Ni^{4+}) = 0.21 Å, which are calculated from 0.545 Å for Co^{3+} [low-spin state (LS), coordination number (CN) = 6], 0.53 Å for Co^{4+} [high-spin state (HS), CN = 6], 0.645 Å for Mn^{3+} (HS, CN = 6), 0.530 Å for Mn^{4+} (HS, CN = 6), Ni^{2+} (CN = 6) and 0.48 Å for Ni^{4+} (LS, CN = 6) [26]. Although the reason for smaller dimensional change of $LiCoMnO_4$ compared with $LiMn_2O_4$ and LiNiMO has yet to be ~~clarified~~, redox couple of Co^{3+}/Co^{4+} plays crucial role upon the high dimensional stability of $LiCoMnO_4$.

High dimensional stability of the $LiCoMnO_4$ electrode including the conductive additive and the polymer binder was confirmed by measuring electrode thickness during cycling. The thickness of the LTO/$LiCoMnO_4$ cell operated at 0.25 mA cm^{-2} in the voltage range from 1.5 to 3.8 V (ca. 3.0–5.3 V of $LiCoMnO_4$ against Li-metal electrode) was measured by a high-precision dilatometer [23]. The thickness changes at 6th to 10th cycles to eliminate the effect of deformation of plastic in a flexible bag cell are shown in Fig. 5b. Since zero-stain lithium insertion material of LTO has no change in electrode thickness [23], change in thickness of the LTO/$LiCoMO_4$ cell measured by the high-precision dilatometer is mainly caused by change in thickness of $LiCoMnO_4$ electrode. As shown in Fig. 5, the $LiCoMnO_4$ electrode expanded and contracted during charge and discharge, respectively, which is well consistent with the change in lattice parameter of $LiCoMnO_4$ during the reactions. The differences in the cell thickness under charged and discharged conditions were almost constant at 0.5–0.6 µm, suggesting that no irreversible deformation ~~happened~~ in the $LiCoMnO_4$ electrode. On the basis of thickness of the $LiCoMnO_4$ electrode in the dry state (106 µm), change in the cell thickness (0.5–0.6 µm) corresponds to 0.5%, which was almost the same as the change in cubic lattice parameter of the $LiCoMnO_4$ observed by XRD measurements. To compare the dimensional stability of the $LiCoMnO_4$ electrode with other lithium insertion elec-

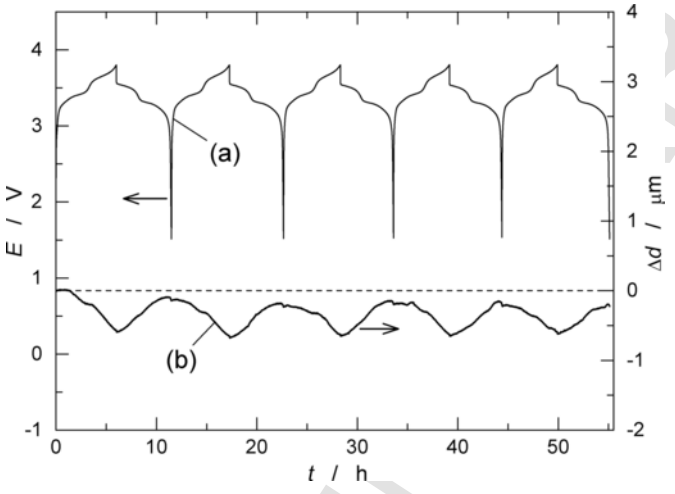

Fig. 5. (a) A charge and discharge curve of an LTO/$LiCoMnO_4$ cell operated in the voltage range from 1.5 to 3.8 V at 0.25 mA cm^{-2} at 25 °C. (b) Change in the cell thickness measured by a precision dilatometer. The thickness of the $LiCoMnO_4$ and LTO electrode were 106 µm (27.7 mg) and 166 µm (47.6 mg), respectively. Shown data were recorded after 5 cycles to eliminate the effect of deformation of plastic in a flexible bag cell.

~~change~~ in electrode thickness of $Li[Ni_{1/2}Mn_{3/2}]O_4$ (LiNiMO) and $Li[Li_{0.1}Al_{0.1}Mn_{1.8}]O_4$ (LAMO) [27] were ~~examined~~ in a lithium-ion cells with the LTO negative electrode (Fig. 6). Both LiNiMO and LAMO electrodes decreased and increased the electrode thickness during lithium extraction and insertion reactions, respectively, as well as the $LiCoMnO_4$ electrode. However, the changes in electrode thickness of LiNiMO and LAMO electrodes were significantly larger than that of the $LiCoMnO_4$ electrode.

Cycle tests were performed with a LTO/$LiCoMnO_4$ cell for 50 cycles (Fig. 7). Almost constant operating voltage during the cycle tests indicates no significant increase of internal resis $CoMnO_4$ cell. Although discharge capacity decr by cycle, 90 mAh g^{-1} was maintained even afte condition of charge-end voltage at 5.35 V again efficiency of the cell, which was low at the ea test, approached to be 100% afterward. At 50th cycle, coulombic efficiency was ca. 94%. Electrolyte instability at high operating voltage (>5 V) results in lower coulombic efficiency due to side reactions, such as electrolyte decomposition. Thus, the coulombic efficiency of $LiCoMnO_4$ relatively lower than those of other 5-V lithium insertion materials such as LiNiMO. The operating voltage of $LiCoMnO_4$ is 0.3 V higher than that of LiNiMO. A comparison of cycleability of cells with $LiCoMnO_4$ in previous reports [17,28,29] revealed that the cell with the well-crystallized $LiCoMnO_4$ exhibited the highest capacity retention and coulombic efficiency, indicating that the high crystallinity with small surface area is crucial to obtain high cycleability of the high-voltage lithium insertion material, $LiCoMnO_4$, as well as LiNiMO [20,21]. Polarization of the cell increases during the cycle test, leading to the capacity loss after 50 cycles corresponding to ~13% of initial capacity. The prolonged cycle tests of $LiCoMnO_4$ were disturbed by problems relating to electrolyte instability, such as formation of a polymer film with high resistance, as reported previously [30,31]. Electrolyte with a large voltage window especially at high voltage region should be developed to evaluate further cycling stability of the $LiCoMnO_4$. The $LiCoMnO_4$ with high dimensional stability could be an excellent electrode for lithium-ion ~~battery~~ with solid electrolyte.

4. Conclusions

As a potential positive electrode of Li-ion batteries with long life cycle, $LiCoMnO_4$ was prepared by the two-step solid-state reaction. The XRD examinations showed small change, only 0.7%, in the lattice parameters of $LiCoMnO_4$ after charged and discharged states. The change was one-third of other lithium insertion materials having spinel-framework structure. According to dilatometry of the $LiCoMnO_4$ electrode, change in electrode thickness was very small and highly reversible. However, cycle tests of the LTO/$LiCoMnO_4$ cell resulted in 13% capacity loss after 50 cycles because of instability of organic electrolytes at high operation voltage of $LiCoMnO_4$ (5 V). $LiCoMnO_4$ would be a promising positive electrode combined with more stable electrolytes at high operation voltage, such as solid electrolytes in all-solid-state lithium-ion batteries in future.

Acknowledgement

This work was partly supported by Advanced Low Carbon Technology Research and Development Program, Specially Promoted Research for Innovative Next Generation Batteries (ALCA Spring) from the Japan Science and Technology Agency (JST), Japan.

課題番号

LiNiMO should be in the same line. Do not separate "Ni".

changes

delete "a"

confirmed

fully clarified

This sentence should be moved in front of the previous sentence (Thus,...).

occurred

batteries

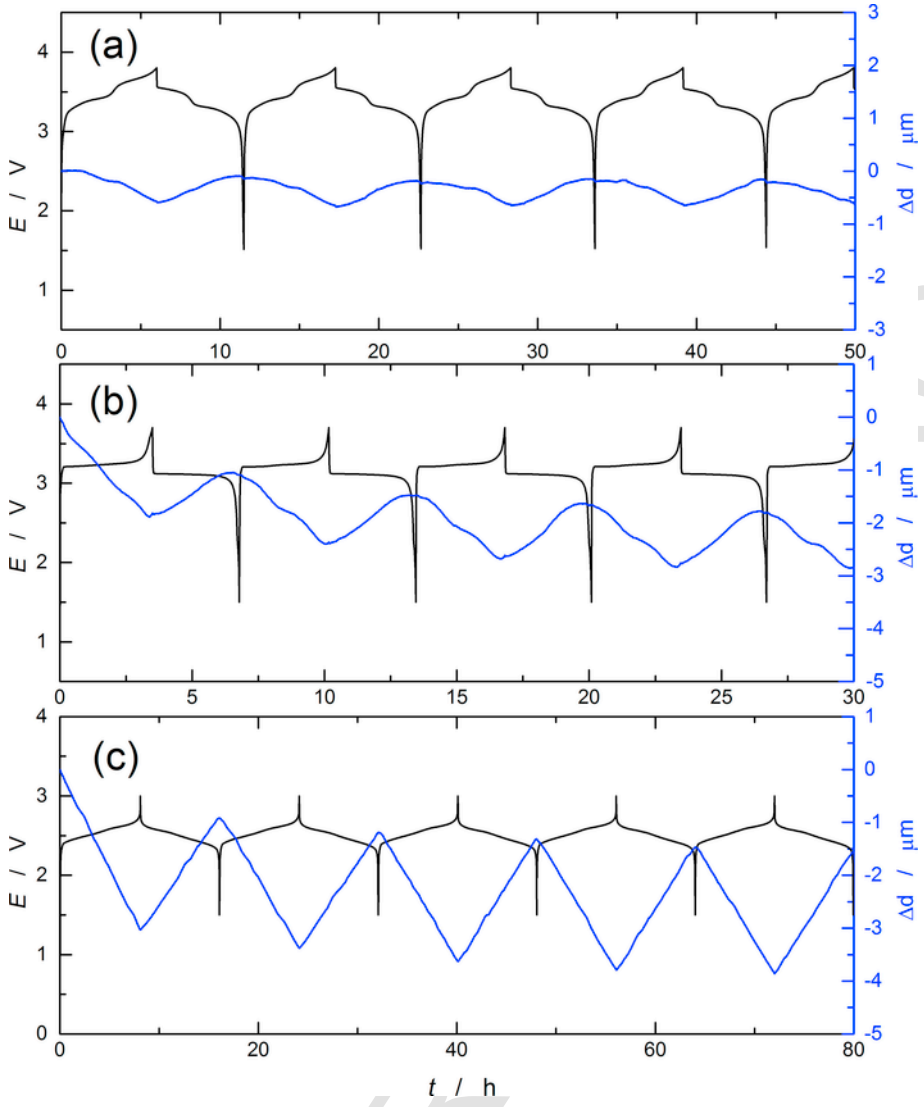

Fig. 6. Thickness of (a) $LiCoMnO_4$, (b) $Li[Ni_{1/2}Mn_{3/2}]O_4$, and (c) $Li[Li_{0.1}Al_{0.1}Mn_{1.8}]O_4$ electrodes measured by the high precision dilatometer during charge and discharge. The zero-strain lithium insertion electrode of LTO was used as a negative electrode. The cells were operated at 0.25 mA cm^{-2} at 25 °C. The electrode weight and thickness were 27.7 mg and 106 μm for $LiCoMnO_4$, 28.1 mg and 92.5 μm for $Li[Ni_{1/2}Mn_{3/2}]O_4$, and 37.4 mg and 151 μm for $Li[Li_{0.1}Al_{0.1}Mn_{1.8}]O_4$ electrode. The 6th to 10th cycles were shown.

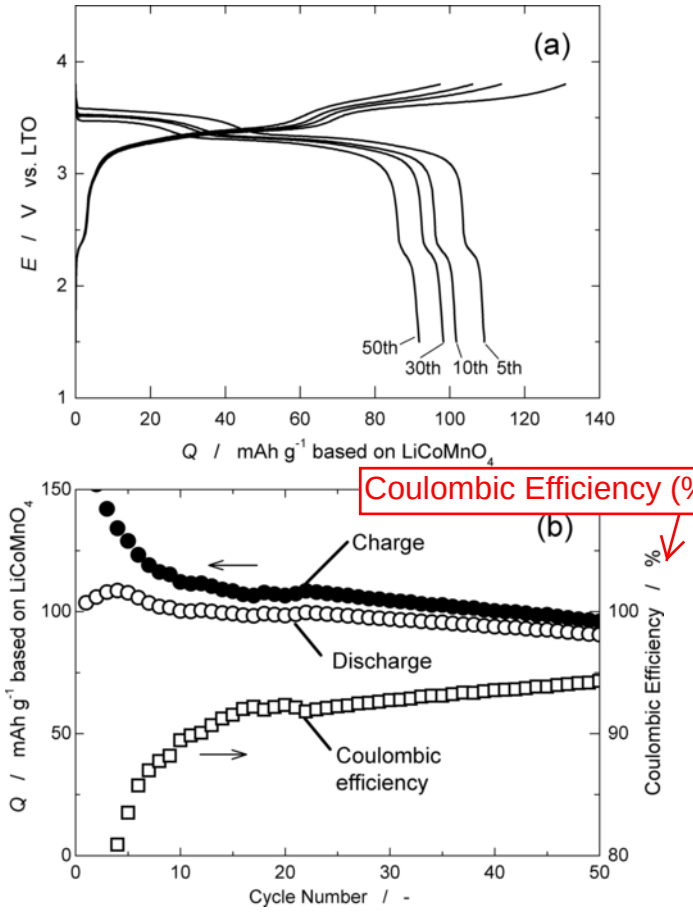

Fig. 7. (a) Charge and discharge curves and (b) charge and discharge capacities and coulombic efficiency of an LTO/$LiCoMnO_4$ cell operated at 0.25 mA cm^{-2} in the voltage range from 1.5 to 3.8 V during the cycle test.

References

[1] P. Yan, J. Zheng, M. Gu, J. Xiao, J.G. Zhang, C.M. Wang, Intragranular cracking as a critical barrier for high-voltage usage of layer-structured cathode for lithium-ion batteries, Nat. Commun. 8 (2017) 14101.

[2] A. Mukhopadhyay, B.W. Sheldon, Deformation and stress in electrode materials for Li-ion batteries, Prog. Mater. Sci. 63 (2014) 58–116.

[3] A. Ulvestad, A. Singer, J.N. Clark, H.M. Cho, J.W. Kim, R. Harder, J. Maser, Y.S. Meng, O.G. Shpyrko, Topological defect dynamics in operando battery nanoparticles, Science 348 (2015) 1344–1347.

[4] D. Wang, X. Wu, Z. Wang, L. Chen, Cracking causing cyclic instability of $LiFePO_4$ cathode material, J. Power Sources 140 (2005) 125–128.

[5] C.Y. Chen, T. Sano, T. Tsuda, K. Ui, Y. Oshima, M. Yamagata, M. Ishikawa, M. Haruta, T. Doi, M. Inaba, S. Kuwabata, In situ scanning electron microscopy of silicon anode reactions in lithium-ion batteries during charge/discharge processes, Sci. Rep. 6 (2016) 36153.

[6] J. Christensen, J. Newman, Stress generation and fracture in lithium insertion materials, J. Solid State Electrochem. 10 (2006) 293–319.

[7] J. Li, N. Lotfi, R.G. Landers, J. Park, A single particle model for lithium-ion batteries with electrolyte and stress-enhanced diffusion physics, J. Electrochem. Soc. 164 (2017) A874–A883.

[8] R. Purkayastha, R. McMeeking, Stress due to the intercalation of lithium in cubic-shaped particles: a parameter study, Meccanica 51 (2016) 3081–3096.

[9] N. Yabuuchi, T. Ohzuku, Solid-state chemistry and electrochemistry of $LiCo_{1/3}Ni_{1/3}Mn_{1/3}O_2$ for advanced lithium-ion batteries, II. Preparation and characterization, J. Power Sources 146 (2005) 636–639.

[10] T. Ohzuku, A. Ueda, N. Yamamoto, Zero-strain insertion material of $Li[Li_{1/3}Ti_{5/3}]O_4$ for rechargeable lithium cells, J. Electrochem. Soc. 142 (1995) 1431–1435.

[11] K. Ariyoshi, R. Yamato, T. Ohzuku, Zero-strain insertion mechanism of $Li[Li_{1/3}Ti_{5/3}]O_4$ for advanced lithium-ion (shuttlecock) batteries, Electrochim. Acta 51 (2005) 1125–1129.

[12] H.-G. Jung, M.-W. Jang, J. Hassoun, Y.-K. Sun, B. Scrosati, A high-rate long-life $Li_4Ti_5O_{12}/Li[Ni_{0.45}Co_{0.1}Mn_{1.45}]O_4$ lithium-ion battery, Nat. Commun. 2 (2011) 516.

[13] N. Yabuuchi, Y. Makimura, T. Ohzuku, Solid-state chemistry and electrochemistry of $LiCo_{1/3}Ni_{1/3}Mn_{1/3}O_2$ for advanced lithium-ion batteries, III. Rechargeable capacity and cycleability, J. Electrochem. Soc. 154 (2007) A314–A321.

[14] Y. Kato, S. Hori, T. Saito, K. Suzuki, M. Hirayama, A. Mitsui, M. Yonemura, H. Iba, R. Kanno, High-power all-solid-state batteries using sulfide superionic conductors, Nature Energy 1 (2016) 16030.

[15] A. Sakuda, T. Takeuchi, M. Shikano, H. Sakaebe, H. Kobayashi, High reversibility of "soft" electr… gy Res. 4 (2016) 19.

checkしてください。

[16] C.W. Sun, J. Liu, Y.D. Gong, D.P. Wilkinson, J.J. Zhang, Recent advances in all-solid-state rechargeable lithium batteries, Nano Energy 33 (2017) 363–386.

[17] R. Alcantara, M. Jaraba, P. Levela, J.L. Tirado, Electrochemical, ^6Li MAS NMR, and X-ray and neutron diffraction study of $LiCo_xFe_yMn_{2-(x+y)}O_4$ spinel oxides for high-voltage cathode materials, Chem. Mater. 15 (2003) 1210–1216.

[18] H. Kawai, M. Nagata, H. Tsukamoto, A.R. West, A new lithium cathode $LiCoMnO_4$: toward practical 5 V lithium batteries, Electrochem, Solid State Lett. 1 (1998) 212–214.

[19] H. Kawai, M. Nagata, H. Kageyama, H. Tukamoto, A.R. West, 5 V lithium cathodes based on spinel solid solutions $Li_2Co_{1+x}Mn_{3-x}O_8$: -1 < x < 1, Electrochim. Acta 45 (1999) 315–327.

[20] K. Ariyoshi, Y. Iwakoshi, N. Nakayama, T. Ohzuku, Topotactic two-phase reactions of $Li[Ni_{1/2}Mn_{3/2}]O_4$ ($P4_332$) in nonaqueous lithium cells, J. Electrochem. Soc. 151 (2004) A296–A303.

[21] Y. Maeda, K. Ariyoshi, T. Kawai, T. Sekiya, T. Ohzuku, Effect of deviation from Ni/Mn Stoichiometry in $Li[Ni_{1/2}Mn_{3/2}]O_4$ upon rechargeable capacity at 4.7 V in nonaqueous lithium cells, J. Ceram. Soc. Jpn. 117 (2009) 1216–1220.

[22] K. Ariyoshi, Y. Maeda, T. Kawai, T. Ohzuku, Effect of primary particle size upon polarization and cycling stability of 5-V lithium insertion material of $Li[Ni_{1/2}Mn_{3/2}]O_4$, J. Electrochem. Soc. 158 (2011) A281–A284.

[23] M. Nagayama, K. Ariyoshi, Y. Yamamoto, T. Ohzuku, Characterization of lithium insertion electrodes by precision dilatometer: area-specific deformation of single electrode, J. Electrochem. Soc. 161 (2014) A1388–A1393.

[24] N. Reeves-McLarren, J. Sharp, H. Beltran-Mir, W.M. Rainforth, A.R. West, Spinel-rock salt transformation in $LiCoMnO_{4-\delta}$, Proc. R. Soc. A 472 (2015) 20140991.

[25] T. Ohzuku, M. Kitagawa, T. Hirai, Electrochemistry of manganese dioxide in lithium nonaqueous cell III. X-ray diffractional study on the reduction of spinel-related manganese dioxide, J. Electrochem. Soc. 137 (1990) 769–775.

[26] R.D. Shannon, Revised effective ionic radii and systematic studies of interatomic distances in halides and chaleogenides, Acta Crystallogr. A 32 (1976) 751–767.

[27] K. Ariyoshi, E. Iwata, M. Kuniyoshi, T. Ohzuku, Lithium aluminum manganese oxide having spinel-framework structure for long-life lithium-ion batteries, Electrochem. Solid State Lett. 9 (2006) A557–A560.

[28] M. Hu, Y. Tian, J. Wei, D. Wang, Z. Zhou, Porous hollow $LiCoMnO_4$ microspheres as cathode materials for 5 V lithium ion batteries, J. Power Sources 247 (2014) 794–798.

[29] A. Windmuller, C.-L. Tsai, S. Moller, M. Balski, Y.J. Sohn, S. Uhlenbruck, O. Guillon, Enhancing the performance of high-voltage $LiCoMnO_4$ spinel electrodes by fluorination, J. Power Sources 341 (2017) 122–129.

[30] P. Arora, R.E. White, M. Doyle, Capacity fade mechanisms and side reactions in lithium-ion batteries, J. Electrochem. Soc. 145 (1998) 3647–3667.

[31] J. Vetter, P. Novák, M.R. Wagner, C. Veit, K.-C. Möller, J.O. Besenhard, M. Winter, M. Wohlfahrt-Mehrens, C. Vogler, A. Hammouche, Ageing mechanisms in lithium-ion batteries, J. Power Sources 147 (2005) 269–281.